IEEE Access
Multidisciplinary ⋮ Rapid Review ⋮ Open Access Journal

Received 31 March 2025, accepted 10 April 2025, date of publication 16 April 2025, date of current version 25 April 2025.

Digital Object Identifier 10.1109/ACCESS.2025.3561607

RESEARCH ARTICLE

CSMA: A Standalone and ImageJ-Compatible Tool for Enhanced Wound Healing Assay Analysis

TRI THANH PHAM[1], AMINA SAGYMBAYEVA[1], TIMUR ELEBESSOV[1], ZHADYRA ONZHANOVA[2], AND FERDINAND MOLNÁR[2], (Associate Member, IEEE)

[1]Laboratory of Mechanobiology, Nazarbayev University, 010000 Astana, Kazakhstan
[2]Laboratory of Cell Growth Regulation, Department of Biology, School of Sciences and Humanities, Nazarbayev University, 010000 Astana, Kazakhstan

Corresponding authors: Tri Thanh Pham (tri.pham@nu.edu.kz) and Ferdinand Molnár (ferdinand.molnar@gmail.com)

This work was supported in part by Ministry of Science and Higher Education of the Republic of Kazakhstan Grant # AP23487220 and in part by the Nazarbayev University Collaborative Research Proposal # 091019CRP2108.

ABSTRACT Accurate quantification of wound closure in cell migration assays is crucial yet challenging. Still, existing methods often underperform due to omitting cell detection within the wound area, resulting in biased outcomes. We developed the CSMA standalone and ImageJ-compatible tool, which utilizes advanced image processing techniques, including contrast enhancement, edge detection, and morphological operations, to precisely identify and quantify cells in the wound region. CSMA offers user-friendly features and adjustable parameters to accommodate different imaging conditions, ensuring robust performance across diverse experimental setups. Validation against conventional tools confirms CSMA's superior ability to delineate wound boundaries and provide accurate estimations of area and width at every time point. As applied to SW480-ADH colon cancer cells treated with various compounds, CSMA proves valuable in biomedical research. CSMA represents a significant advancement in wound healing assay analysis, providing researchers with a simple and reliable tool for studying cell migration dynamics with enhanced precision and reproducibility. CSMA is available as a standalone and ImageJ-compatible tool with its source code at https://github.com/AminaSagymbayeva/CSMA_WoundHealing

INDEX TERMS Cell migration, wound healing, scratch assay, analysis tool, advanced image processing, ImageJ integration.

I. INTRODUCTION

Wound healing assay is a classic method for the assessment of collective cell movement in epithelial and endothelial tissue cultures [1]. It can be applied to study persistence, speed, and the effect of cell-to-cell and cell-to-extracellular matrix interactions in populations of migrating cells [1], [2], [3]. Moreover, it may be coupled with different microscopy methods to study intracellular events that occur during migration [1]. Wound healing assay is often a method of choice because of its compatibility with multiple cell lines, easy and inexpensive setup, and wide application [4]. Therefore, it is used as a model for studying many processes, such as embryonic morphogenesis, angiogenesis, *in vivo* wound healing, and metastasis [5], [6], [7], [8], [9].

Migrating cell cohorts maintain their intercellular junctions, unlike individual migrating cells [7]. Cell-cell junctions are supported by adherens junction proteins that interact with actin cytoskeleton and allow cell plasticity [7]. In epithelial cells, cadherins, specifically E-cadherin (*CDH1*), play a central role in cell-cell adhesion and supracellular polarization [3], [7]. Cell polarization is induced by extracellular chemical signals, such as growth factors, cytokines, and extracellular ligands [3], [7]. In response to chemical stimuli, the actin cytoskeletons in cells at the leading edge reorganize to form various protrusions, such as broad lamellipodia and cylindrical filopodia [3], [7]. Interestingly, not only do the cells at the front of the edge develop protrusions, but also those behind them form 'cryptic' lamellipodia to interact

The associate editor coordinating the review of this manuscript and approving it for publication was Sandra Costanzo.

with the substratum and thus promote further movement [10]. Four small GTPases – Rho, Rac, Ras, and Cdc42 – are the dominant regulators of the collective cell movement, as they control many processes from cell polarization to adhesion, to pseudopodia development [4].

Wound healing assay includes growing cells of interest to high-level confluency, creating a narrow gap in the tissue monolayer, and taking snapshots of it at equal time intervals to observe the gap closure [1]. There are two methods of gap introduction: physical exclusion and direct manipulation [2]. The first method prevents monolayer growth under an insert placed in the dish. Although it is more expensive, this method causes less damage to cells at the gap front and produces a cleaner gap with less debris [2]. The second method, commonly referred to as the scratch assay, is more popular due to its cost efficiency and ease of implementation. A gap is created by scratching the surface of the tissue monolayer with a sharp object, such as a micropipette tip [1]. Subsequently, a time-lapse series of images is captured to monitor and estimate the rate of gap closure [2].

Conventionally, each snapshot image is analyzed manually [2]. However, this method is very time-consuming and prone to user bias. Several plugins, scripts, and stand-alone software have been developed for the automatic or semi-automatic quantification of wound closure. Many of them demonstrate highly accurate wound detection on images with different illumination conditions and require the adjustment of only a few parameters [11], [12], [13], [14], [15], [16], [17], [18]. However, since some of these algorithms only account for the largest cell-free area, as demonstrated in Fig. 1, they sometimes underestimate the true wound area, especially when it is divided into multiple regions. In addition, they detect only the wound front and ignore cells that are left in the center of the gap, which also introduces a bias in the results as shown in Fig. S1. Though not all cell types tend to break away from the tissue monolayer and migrate inside the gap, for those cell lines that do, the currently available software may produce inaccurate results.

In this paper, we present a newly developed standalone and ImageJ-compatible tool for enhanced wound healing assay analysis named Cell Scratch Migration Analysis (CSMA). We have used ImageJ for the integration of CSMA, a widely used, open-source image processing and analysis software developed by the National Institutes of Health (NIH) [19]. ImageJ provides an extensible platform that enables researchers to develop custom plugins and tools for specific image analysis applications. In our benchmarks, CSMA improves existing tools by (i) enhancing the quantification of the wound closure by detecting the cells found in the middle of the wound, (ii) providing a user-friendly interface, (iii) offering two modes of quantification by wound area closure (hence wound closure from this point on) or by wound width, and (iv) supporting various imaging conditions due to the flexibility in parameter adjustment. We demonstrated the features of the applied CSMA tool on a dataset created by treating SW480-ADH colon cancer cells with weak (WVA) and strong (SVA) vitamin D receptor (VDR) agonists, where WVA is about 10,000 times weaker than SVA. VDR signaling is an excellent model for studying migration because *CDH1*, involved in cell-cell adhesion, is its direct target gene [20]. CSMA is available as a standalone and ImageJ-compatible tool with its source code at https://github.com/AminaSagymbayeva/CSMA_WoundHealing.

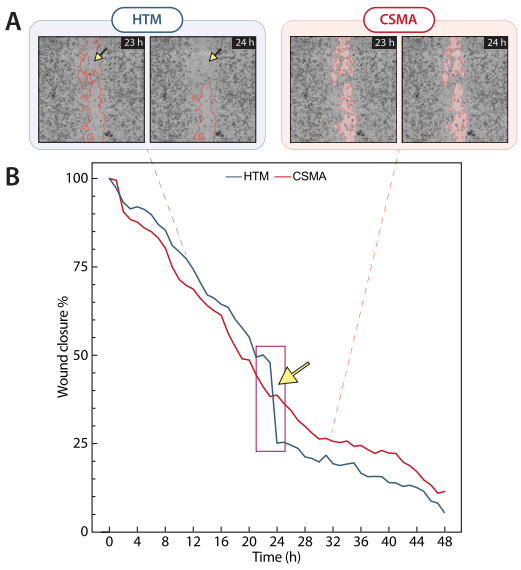

FIGURE 1. Comparison of wound detection between HTM and CSMA. (A) Representative time-series images showing wound closure in SW480-ADH colon cancer cells (solvent control group) as detected by HTM (blue rectangle) and CSMA (red rectangle). Yellow arrows indicate regions that HTM incorrectly dismisses from calculations when the wound gap closes in the middle, which CSMA properly detects and quantifies. (B) Quantitative comparison of wound area percentage over time as tected by HTM (blue line) and CSMA (red line). The yellow arrow points to the artificial rapid drop in wound area percentage at approximately 24 hours in HTM data, resulting from the detection limitation shown in panel A.

II. MATERIALS AND METHODS

A. CELL CULTURE AND MAINTENANCE

The SW480-ADH human colon cancer cell line, which was used to test the CSMA tool, was kindly provided by Professor Alberto Muñoz Terol from CSIC-Autonomous University of Madrid. The SW480-ADH human colon cancer cell line was selected for this study due to its tendency to form individual migrating cells within the wound area, making it ideal for testing CSMA's advanced detection capabilities. Additionally, these cells form consistent monolayers while responding to VDR agonists, which regulate *CDH1* as mentioned earlier, allowing the effective testing and benchmarking of the CSMA tool. The SW480-ADH cells were cultured in Dulbecco's Modified Eagle Medium (DMEM) (high glucose, GlutaMAX, Life Technologies Limited, UK) supplemented with 10% (v/v) fetal bovine serum (FBS, Life Technologies Limited, UK), and 1% (v/v) penicillin-streptomycin (#15140-122, Gibco) at 37ºC in 5% CO_2. Prior to experiments, the cells were cultured for three days, reaching 70% confluency.

Cell viability was determined by trypan blue (cat. no. T10282, Life Technologies Limited, UK) exclusion using Corning hemocytometer Cell Counter (cat no. CLS6749, Corning, Inc, Germany).

B. WOUND HEALING ASSAY

SW480-ADH human colon cancer cells were seeded in a standard 24-well culture plate at a density of 2.5×10^5 cells per well and incubated in $500\mu l$ of DMEM supplemented with 10% (v/v) FBS at 37ºC until they reached the confluency of 90 - 95%. All experiments were performed on cells between passages 4 and 10. A gap in the cell monolayer was introduced using a sterile generic $200\mu l$ micropipette tip. The $200\mu l$ micropipette with a plastic tip was pressed against a plastic ruler pre-sterilized with 70% ethanol solution to make the gap in a straight line at the middle of the well. Subsequently, the growth medium was removed, and the well was gently washed two times with $1\times$ phosphate buffer solution (PBS) to remove detached cells and cell debris. Cells were treated with DMSO as a solvent control, $10nM$ SVA, or $100\mu M$ WVA. Prior to the treatment, both ligands were dissolved in $500\mu l$ DMEM supplemented with 5% FBS. The cells were then incubated at 37ºC in 5% CO_2 for 48 hours. The experiment was performed once with four replicates per condition.

C. DATASETS FOR TESTING AND ANALYSIS

The images were acquired using an Omni Cell Imager Microscope (CytoSMART® Technologies BV, The Netherlands) at $10\times$ magnification. This automated imaging system is specifically designed to maintain consistent image acquisition parameters throughout long-term experiments, compensating for potential shifts and lighting changes that may occur during the 48-hour incubation period. CytoSmart's built-in algorithms ensure uniform imaging conditions across all time points. To further ensure consistency, we prevented the opening of incubator doors during the entire 48-hour imaging period, eliminating potential temperature fluctuations and external light interference that could affect both image quality and cell behavior. The imaging was done at 1-hour intervals over 48 hours. Regions with 1 mm radii were selected from each well at approximately the same position. Regions close to the well periphery were avoided during selection due to poor illumination. A total of 49 images were exported for each condition as JPEG files. Regions with dimensions of approximately 1537×1537 pixels were cropped from the exported files using the ImageJ toolkit.

Additionally, a publicly available dataset, consisting of 48 images of mutant human renal carcinoma cell line, 769-P (ATCC CRL-1933) imaged for 23.5 hours every 30 minutes using the Live Cell-R Station (Olympus), was used for the comparative testing of different wound detection tools [14].

D. DATA ANALYSIS WITH CSMA

The CSMA tool is free and open-source software based on the OpenCV (version 4.7.0.72) library. The applications was developed in both Python 3 and Java programming languages. Python 3 is used for image processing and the user interface (UI), whereas Java facilitates communication between ImageJ and Python.

The image analysis tool is available as the ImageJ integration for Windows and a source code with UI for Linux and macOS. CSMA supports common image extensions such as *.tif, *.jpeg, and *.png and before its usage, the user must configure a virtual environment named ImageJCSMA using an executable file included in the package. All necessary Python libraries are automatically installed in this environment, preventing conflicts with possibly existing library versions on the user's PC.

The image processing algorithm is divided into two stages: i) first mask creation and ii) wound and cell edge detection as summarized in Fig. 2. The first stage creates a mask with roughly defined wound edges, while the second stage refines the wound edges and detects cells within the wound. The algorithm description provided below is applicable with default parameters listed in Table 1.

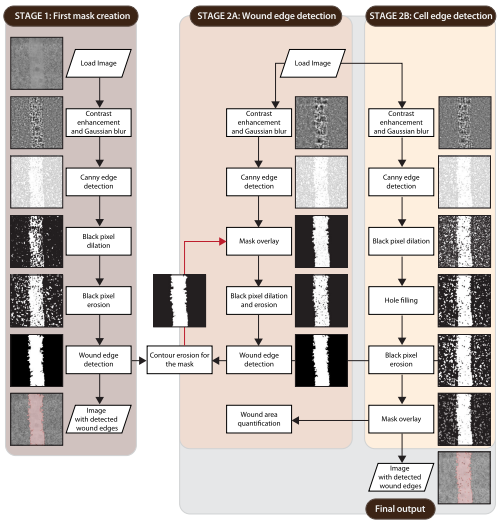

FIGURE 2. Schematic workflow of the CSMA algorithm. The algorithm's two-stage image processing pipeline: Stage 1 creates an initial mask with approximate wound boundaries, while Stage 2 (A and B sub-stages) refines these boundaries and identifies cells within the wound. Representative images showing the progressive transformation of the original image at each processing step using default parameters (SW480-ADH colon cancer cells, solvent control group). The processing pipeline includes contrast enhancement, edge detection using Canny method, morphological operations to connect cell boundaries, and identification of both wound boundaries and cells within the wound area. To avoid terminology confusion, throughout the workflow, "wound edges" are consistently referred to as the detected boundaries.

First, the original image is preprocessed by applying contrast limited adaptive histogram equalization (CLAHE) image contrast enhancement method and Gaussian blurring. Gaussian blurring is achieved by convolving the input image with a Gaussian kernel of 9×9 pixels to remove noise signals. CLAHE is superior to simple histogram equalization since it generates fewer noise signals that may lead to artifacts in the processed image [21]. The CLAHE method enhances local

contrast at cell-covered and cell-free area boundaries, crucial for distinguishing cells with similar intensity to background. Gaussian blurring reduces noise that could cause false edge detection while preserving true wound boundaries. After image preprocessing with CLAHE and Gaussian blurring, wound edges are detected with the Canny edge detection method [22], which performs more reliably on the enhanced input, especially in images with uneven illumination or low contrast. The lower threshold value used to differentiate between candidate edges and true non-edges is calculated with Otsu's method [23], while the higher threshold is fixed at 255.

Since the Canny method detects only individual cells within the cell monolayer on both sides of the wound, the next step is to fuse these individual cell boundaries into continuous wound front. This is done by first expanding the boundaries of the individual cells to merge them and then eroding them back using OpenCV morphological operations. Since users might have images of different sizes and resolutions, the parameters for all morphological operations are adjustable. The perimeter of the image is then padded with one row of black pixels to connect the front cells on two sides of the wound into a single continuous boundary. Lastly, the largest boundary (true wound boundary) filled with white pixels is redrawn on a black background with *cv2.drawCountours* function, creating a wound gap mask. Since morphological operations applied earlier distort the true edges of the wound, the redrawn wound boundary is eroded back to avoid overestimation in the output image.

The same operations are performed in the second stage of image processing. After the Canny edge detection method is applied in the wound edge detection pipeline, the black-and-white binary mask created earlier is overlaid on top of the newly obtained image to ensure that no residual holes remain in the cell monolayer in the output image. Morphological operations are applied as previously, but the parameter values are set lower for a more accurate representation of wound edges. After all boundaries, including true wound bondaries and individual cell boundaries, are detected on the black-and-white image with *cv2.findContours* function, the areas enclosed by these boundaries are calculated. If a boundary-enclosed area is smaller than 100 pixels or its ratio to the largest detected boundary is less than 0.15, it is classified as noise and discarded. The remaining boundaries are redrawn on a black background and filled with white pixels.

Similar steps are repeated to detect cells inside the wound. The output image with refined wound edges is obtained; however, the contrast limit and square grid size values for the CLAHE contrast enhancement function are reduced to minimize noise signals. Finally, the wound edge and cell edge detection pipelines are combined to produce an image with refined wound edges and cells within the wound.

At last, the number of white pixels representing the wound is calculated in the output image. The area of the gap is normalized and converted to the percentage as shown in Equation 1:

$$A_t(\%) = \frac{\mathrm{A}_t(\mathrm{pixel})}{A_0(\mathrm{pixel})} \times 100 \tag{1}$$

where A_t is the total cell-free area at a given time, and A_0 is the initial cell-free area.

The alternate width-based quantification method is also implemented using a similar image processing technique. As shown in Fig. S2, the difference is that the cell edge detection pipeline is removed from the algorithm, which significantly reduces the processing time, and the quantification of the gap width is performed by calculating the number of white pixels in every row. The mean of the gap width for every image is calculated as shown in Equation 2:

$$\mathrm{mean} = \frac{\sum w_i}{n} \tag{2}$$

where w_i is the gap width in i^{th} row, and n is the number of rows.

CSMA produces three types of outputs: a.csv file with the calculated wound area or width for every time point in pixels and percentage formats, output images with detected wound boundaries, and a graph representing the closure of the wound over time.

CSMA effectively handles variations in wound shape and size through several mechanisms. The combination of Canny edge detection with customizable morphological operations adapts to irregular boundaries, while the two-stage processing approach accurately identifies complex or fragmented wound geometries. CSMA's ability to detect cells within the wound area is particularly valuable for analyzing patterns where isolated cells appear in the wound, as shown in Figure 1. Additionally, the adjustable parameters allow fine-tuning for specific experimental conditions, accommodating variations across different cell types and imaging setups.

The images acquired from treating SW480-ADH cells with DMSO, SVA, and WVA were analyzed by applying user-defined parameter values listed in Table 2.

In summary, CSMA's two-stage image processing approach enables accurate wound detection by first creating a rough mask and then refining it to identify both wound edges and cells within the wound, addressing a key limitation of existing analysis tools.

E. DATA ANALYSIS WITH MRI

Montpellier Ressources Imagerie (MRI) is a semi-automatic ImageJ tool for wound healing assay analysis [24]. MRI tool relies on two different methods for image processing and requires the adjustment of four parameters. It can quantify the area of the wound on a time stack sequence of images and store it in a.csv file. Parameters in Table 3 were used for the analysis as indicated in their tutorial [25].

F. DATA ANALYSIS WITH HTM

HTM Wound healing tool is a semi-automatic tool developed by Dr. Ivan Vorobyev's laboratory for the "Scratch" assay

TABLE 1. Default values applied for the adjustable parameters of the CSMA tool. Default parameter values for the CSMA image processing pipeline. The table shows optimized settings for each adjustable parameter across the three main functional components: first mask creation, wound edge detection, and cell edge detection. These parameters control contrast enhancement (CLAHE), boundary modifications (dilation/erosion), and cell identification processes, providing a reliable starting point for most wound healing assay analyses.

Functional step in the pipeline	Parameter	Parameter setting value		
		First mask creation	Wound edge detection	Cell edge detection
Contrast enhancement (CLAHE)	Contrast limit	30	30	20
	Square grid size	30	30	20
Boundary dilation	Disk radius	5	5	3
	Iterations	2	1	-
Boundary erosion	Disk radius	5.5	5.5	3
	Iterations	2	1	-
Mask erosion	Disk radius	5.5	-	-
	Iterations	2	-	-
Threshold	-	-	0.15	-
Cell filling	Kernel size	-	-	25

TABLE 2. User-defined parameter values applied for wound closure analysis across experimental conditions. The table details the specific parameters used for each replicate (1-4) of SW480-ADH cells treated with DMSO, WVA, or SVA. Bold values indicate parameters that were adjusted from default settings to optimize detection accuracy. This parameter optimization demonstrates CSMA's flexibility in accommodating varying image characteristics across different experimental conditions. For a more detailed description of each parameter and its role in image processing, refer to Supplementary Table S2.

Treatment	DMSO				WVA				SVA			
Replicate	1	2	3	4	1	2	3	4	1	2	3	4
First mask creation												
Contrast limit	**5**	**5**	**10**	**1**	**10**	**10**	**5**	**10**	**5**	**10**	**5**	**5**
Square grid size	30				30				30			
Dilation radius	5	**4**	5	5	**7**	**7**	5	**7**	5	5	5	5
Iterations	2				2				2			
Erosion radius	5.5				5.5				5.5			
Iterations	2				2				2			
Mask erosion radius	**7**	**5**	**5**	**10**	5.5	5.5	**15**	**10**	**10**	**15**	**13**	15
Iterations	**1**				2	2	**3**	**3**	**3**			
Wound edge detection												
Contrast limit	**5**	**5**	**10**	30	**13**	**13**	**5**	**13**	**5**	**10**	**15**	**13**
Square grid size	30				30				30			
Dilation radius	**4**	**4**	5	**6**	**7**	**7**	**8**	**7**	**6**	**7**	**9**	5
Erosion radius	5.5	5.5	**7.5**	**6.5**	5.5	5.5	**6**	5.5	5.5	5.5	**9.5**	5.5
Threshold	0.15	0.15	0.15	**0.1**	0.15				0.15			
Cell edge detection												
Contrast limit	**5**	**8**	**5**	**5**	**15**	**30**	**8**	**15**	**10**	**5**	**10**	**5**
Square grid size	**30**				**30**	**10**	**25**	**30**	**5**	**30**	**30**	**30**
Dilation radius	3				3	3	**4**	3	3			
Erosion radius	3				**6**	**4.5**	3	**4.5**	3			
Cell filling	25	25	**10**	**15**	**15**	25	**10**	**15**	**30**	**10**	**10**	**10**

analysis. It is available in MatLab with no UI. Default parameters were used for the analysis. For demonstration purposes, the code was modified by changing the color and increasing the thickness of the detected boundaries in output images.

G. DYNAMICS OF WOUND CLOSURE

The dynamics of wound closure were initially assumed to be linear with a linear regression line fitted to all time points on the wound closure curve over 48 hours. The gradient or slope of this trendline was used to represent the wound closure rate, expressed as a percentage per hour.

Although linear dynamics of wound closure were observed for all detection methods, this pattern held true only for the early stages of wound closure. Careful observation revealed that the wound closure rate slowed down in the later stages (starting around 30 hours), deviating from the initial linear trend (see Fig. 1 and Fig. 4 for more details). Consequently, the dynamics of wound closure appeared to follow an exponential decay function rather than a linear curve. To better capture this behavior, a single exponential

TABLE 3. Settings used for the MRI ImageJ macro in comparative wound healing assay analysis. These recommended settings from the MRI documentation were applied to ensure fair comparison with CSMA performance. The variance-based method with specified filtering and threshold parameters was selected as the optimal approach for detecting wound boundaries in the test datasets.

Parameter	Value
Method	Variance
Variance filter radius	10
Threshold	50
Radius open	4
Min. size	10 000

decay curve:

$$y = Ae^{-\lambda t} \tag{3}$$

was used to estimate the dynamics of wound closure with λ representing the rate constant or decay constant. The comparison of its suitability against the linear model is shown in Fig. S4.

The statistical methods used to evaluate wound closure rates were selected based on both mathematical fit and biological relevance. Linear regression was initially applied as it provides a straightforward measure of closure rate (percentage per hour), which is easily interpretable and commonly used in the field. However, as shown in Fig. S4, the exponential decay model consistently provided superior fit to the experimental data (higher R^2 values), particularly for later time points. This improved mathematical fit reflects the biological reality of wound closure dynamics, where closure rates typically decrease as available space diminishes and cell-cell contact inhibition becomes more prevalent. The exponential decay constant (λ) thus offers a more accurate representation of the overall closure process, capturing both the initial rapid migration phase and the later deceleration phase in a single parameter. While λ effectively describes the rate of wound closure, it can be less intuitive for biological interpretation. A more commonly used metric in biological systems is the half-life ($t_{1/2}$), which represents the time needed for the wound area to decrease to half of its initial size. This measure is directly related to λ by:

$$t_{1/2} = \frac{\ln 2}{\lambda} \approx \frac{0.693}{\lambda} \tag{4}$$

Using $t_{1/2}$ allows for easier comparison across different experimental conditions, similar to its widespread use in pharmacokinetics and enzyme kinetics.

III. RESULTS

A. EVALUATION OF THE CSMA TOOL WITH DEFAULT AND USER SETTINGS

Solvent-treated group of SW480-ADH cells was used to assess the accuracy of wound detection with the CSMA tool. The default parameters were tested against user-defined parameters, which were tuned according to the instructions provided in the README file. As shown in Fig. 3, the number of cells found in the middle of the wound increased until they fused with the cells at the wound front after approximately 20 hours. The CSMA tool successfully detected the cells in the middle of the gap at all time points, which allowed for more accurate area estimation. The final wound area was estimated to be 11.52% of the initial area (Fig. 3 and 4). The linear wound closure rate estimated for 48 hours was 1.83% per hour ($R^2 = 0.95$). However, when two separate linear regressions were applied to two different regions of the graph with visually distinct wound closure rates, the following values were obtained: 2.48% per hour ($R^2 = 0.99$) for the first 30 hours and 0.90% per hour ($R^2 = 0.90$) for the remaining 18 hours (Fig. 4). The best-fitted exponential decay constant for the entire 48-hour period was 0.043 ($R^2 = 0.98$).

As mentioned earlier, for a more intuitive interpretation of the closure rate, we also report the corresponding half-life ($t_{1/2}$), defined as the time required for the wound area to reduce by 50%. Half-life is widely used in biological sciences, including cell migration and cancer biology, to describe dynamic processes such as drug clearance, tumor growth, and cell population decay [26], [27]. Reporting $t_{1/2}$ makes it easier to compare wound closure kinetics across different experimental conditions in a way that is more intuitive for researchers in life sciences. The calculated values are summarized in Table S1 in the supplementary data. For instance, for $\lambda = 0.043$, the corresponding $t_{1/2}$ is approximately 16.1 hours.

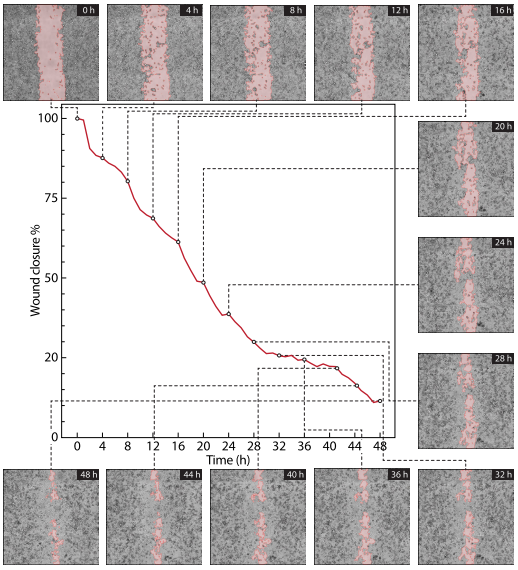

FIGURE 3. Performance of CSMA with default settings. Time-series images showing wound closure in SW480-ADH colon cancer cells (solvent control group) with CSMA-detected boundaries highlighted in red. Quantitative analysis of wound closure over time, automatically generated by the CSMA algorithm. The graph demonstrates consistent wound area detection throughout the experiment, with smooth progression that accurately reflects the biological closure process without artificial discontinuities.

User manipulation of the CSMA settings involved changing the contrast limits only since it was sufficient to achieve

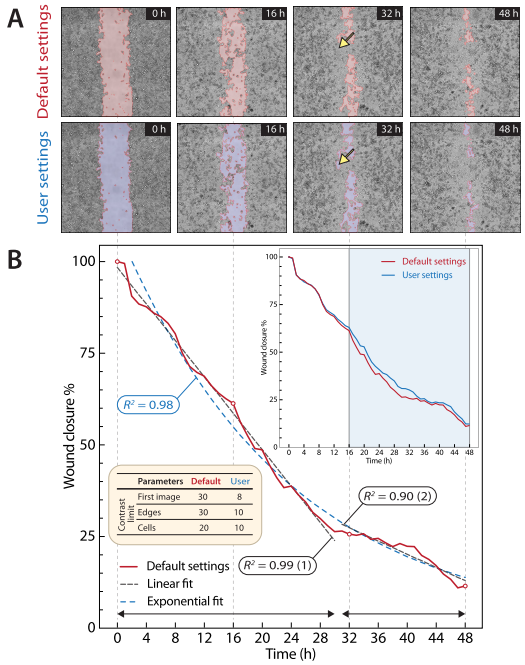

FIGURE 4. Comparison of CSMA performance with default versus user-defined settings. (A) Representative images of wound closure in SW480-ADH cells at key timepoints, showing detection boundaries with default parameters (red) and user-defined parameters (blue). Yellow arrows indicate areas where default settings overestimate cell-covered regions. (B) Quantitative comparison of wound area closure over time with both parameter sets. The inset (blue shaded area) highlights divergence between the two parameter sets after 16 hours, when cells in the wound center begin to merge with the wound front. The table within the graph displays the specific parameter adjustments made. The superior fit of the exponential model (blue dashed line) compared to linear models (black dashed lines) demonstrates the non-linear nature of wound closure dynamics.

reliable quality of wound closure detection as demonstrated in Fig. 4. The final wound area as estimated with user-defined settings was 12.33%, which was slightly larger than with the default settings. The exponential decay rate reduced to 0.041 ($R^2 = 0.99$).

During the first 16 hours, the wound area estimations obtained with default and user-defined parameters correlated closely since cells at the wound front moved uniformly, and cells in the middle of the wound remained separated from the wound front (Fig. 4). However, after 16 hours, the wound front came into proximity to the cells in the middle. The fusion of two wound fronts with cell-covered patches inside the wound led to an overestimation of the covered area for default settings. However, adjusting the contrast limit parameters minimized the area of regions falsely detected (Fig. 4A, yellow arrows).

B. PERFORMANCE COMPARISON OF CSMA, MRI, AND HTM ALGORITHMS

To ensure a fair comparison between all analysis tools, we applied the recommended settings from the provided documentation for each method. For MRI, we used the parameters specified in their tutorial (Table 3), and for HTM, we used the default parameters as provided in the source code. This approach avoids potential bias that might result from custom optimization of one tool over others.

To test the effectiveness of CSMA compared to other publicly available tools for wound healing assay, we selected MRI and HTM. To ensure a fair comparison between all the tools, we applied the recommended settings from the provided README file or source code for each one (Fig. 5). An additional dataset of 769-P cells was chosen to ensure that our tool worked properly on images with different characteristics (Supplementary Fig. S3).

Fig. 5A highlights differences in how cell boundaries were detected by different algorithms. While both HTM and MRI had some challenges in detecting cells at the center of the wound area (yellow arrows), CSMA detected these cells with high precision (green arrow). Further, HTM and MRI could not detect the empty regions in the middle of the wound after 32 hours (blue arrows), leading to biased wound area estimations. In contrast, our tool accurately detected these regions (red arrows). CSMA showed a smaller initial wound area compared to HTM because it successfully detected the cells inside the wound (Fig. 5B). On the other hand, MRI demonstrated a smaller initial wound area than CSMA presumably because of the overestimation of the wound front (see Fig. 5A). Finally, CSMA produced a much smoother wound closure curve than HTM, which falsely detected only the largest remaining wound region as the true wound at approximately 24 hours neglecting the smaller unoccupied areas (Fig. 5B and C).

CSMA also effectively detected wound boundaries and cells within the wound in the 769-P dataset (Supplementary Fig. S3), accurately tracking the migration of cells within the wound. The wound area estimations of CSMA and HTM correlated very closely, except for the sudden drop at 22 hours detected by HTM, which was caused by the disconnected detection of the wound area while only the largest area was used for the estimation. MRI underestimated the area of the wound at all times most probably due to the specificities of the detection algorithm.

In general, CSMA accurately detected cells within the wound in three replicates of SW480-ADH colon cancer cells treated with DMSO. The mean R^2 values obtained from three replicates for the exponential best-fit curves for CSMA, HTM, and MRI were 0.97±0.01%, 0.95±0.03%, and 0.91±0.08%, respectively (see Supplementary Fig. S4). As a result, the wound closure curve of CSMA fitted the exponential model better than that of HTM and MRI as demonstrated by the calculated R^2 values.

C. EFFECT OF SVA AND WVA ON THE MIGRATION OF SW480-ADH CELLS

The effect of SVA and WVA on the migration of human colon cancer cells was assessed by CSMA (Fig. 6A). SW480-ADH cells treated with 100μM WVA demonstrated the lowest mean linear wound closure rate of 0.78 ± 0.22 % per hour (R^2 = 0.93 ± 0.05), compared to 1.17 ± 0.30 % per hour

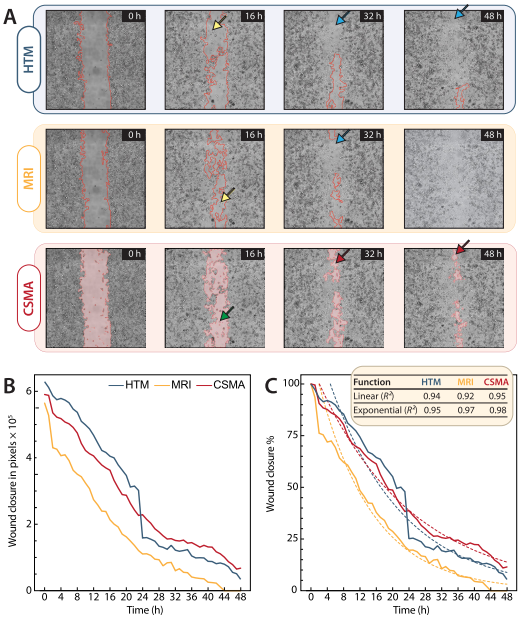

FIGURE 5. Comprehensive comparison of wound detection performance across analysis tools. (A) Representative time-series images showing wound closure in SW480-ADH cells (vehicle control group) as detected by HTM MATLAB code, MRI ImageJ macro, and CSMA. Yellow arrows indicate cells within the wound that HTM and MRI fail to detect, while the green arrow shows CSMA's successful detection of these cells. Blue arrows indicate empty regions that HTM and MRI inaccurately classify as cell-covered after 32 hours, while red arrows point to the same regions that CSMA correctly identifies as still empty. (B) Quantification of absolute wound area (pixels) over time by each method. (C) Normalized wound area closure (percentage) over time. The table shows R^2 values for both linear and exponential model fits, demonstrating CSMA's superior accuracy in capturing wound closure dynamics.

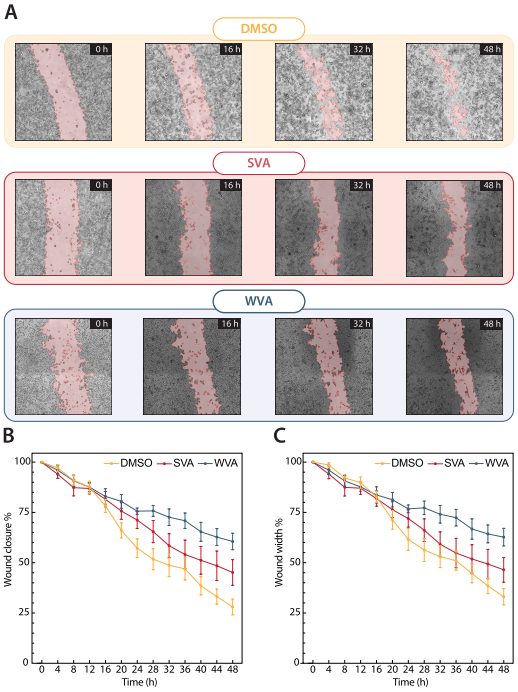

FIGURE 6. Effect of VDR agonists on SW480-ADH cell migration as quantified by CSMA. (A) Representative time-series images showing wound closure in cells treated with DMSO (control), 10nM SVA, or 100μM, with CSMA-detected boundaries highlighted and user-defined parameters listed in Table2. (B) Quantification of mean wound area closure over 48 hours from four independent replicates per treatment, showing dose-dependent inhibition of migration by VDR agonists. (C) Alternative quantification using mean wound width measurements over time, confirming the migration inhibitory effect observed in the area-based analysis.

($R^2 = 0.98 \pm 0.01$) in the group treated with 10 nM SVA, and 1.63 ± 0.21 % per hour ($R^2 = 0.96 \pm 0.02$) in the solvent control group. The mean exponential decay constants obtained from four replicates were estimated as follows: $1.03 \times 10^{-2} \pm 3.30 \times 10^{-3}$ ($R^2 = 0.93 \pm 0.06$) for WVA, $1.78 \times 10^{-2} \pm 8.18 \times 10^{-3}$ ($R^2 = 0.97 \pm 0.01$) for SVA, and $2.83 \times 10^{-2} \pm 6.99 \times 10^{-3}$ ($R^2 = 0.96 \pm 0.02$) for the solvent control group. The average final wound areas were 27.22 ± 8.25 %, 45.20 ± 12.74 %, and 59.89 ± 8.22 % for the DMSO, SVA, and WVA groups, respectively (Fig. 6B).

These results indicate that both SVA and WVA inhibit the migration of SW480-ADH cells in a concentration-dependent manner, with WVA showing stronger inhibitory effects despite its weaker receptor agonist activity. CSMA's precise detection capabilities were essential for accurately quantifying these differences, particularly in later timepoints when cells within the wound area significantly affected closure measurements.

IV. DISCUSSION

The CSMA tool demonstrated high-precision edge detection in all tested datasets by detecting migrating cells in the middle of the wound and minimizing the overestimation of wound edge boundaries. Table 4 summarizes the key features and performance metrics of CSMA compared to existing wound healing assay analysis tools (HTM and MRI), highlighting its advantages in detection accuracy, processing speed, and analytical flexibility.

The performance of CSMA with default and user-defined parameters was comparable, and the final wound area estimations for both vehicle control group SW480-ADH and 769-P cells were less than 1% difference, demonstrating high compatibility of the default parameters with different imaging conditions. However, with user-defined parameters, the wound closure was more accurate in the vehicle control group SW480-ADH since the false detection of empty regions was minimized. Importantly, such improvement in wound detection resulted from the adjustment of only the contrast limits, while the rest of the parameters remained the same. In all analyzed datasets, the user-defined contrast limits of wound edge detection and first mask contrast limit values matched closely, which is why keeping these two parameters the same is a good starting point for fine-tuning the CSMA's settings as listed in Tables 1 and 2.

The detection of cells in the middle of the wound was precise for both the SW480-ADH and 769-P datasets. For instance, CSMA accurately detected the changing boundaries of a migrating cell front in the 769-P dataset with default settings (Supplementary Fig. S3). This suggests that the default parameters of the CSMA tool may serve as a universal

TABLE 4. Comparison of CSMA with existing wound healing assay analysis tools.

Feature	Tool		
	CSMA	HTM	MRI
Detection Capabilities			
Detection of cells within wound area	Yes	No	No
Recognition of disconnected wound regions	Yes	Limited (largest only)	Limited
Detection of irregularly shaped wounds	High accuracy	Moderate	Moderate
Analysis Methods			
Available quantification methods	Area and width-based	Area-based only	Area-based only
Exponential fit accuracy (R^2)	0.97 ± 0.01	0.95 ± 0.03	0.91 ± 0.08
Processing speed (seconds/image)	$2.26 \times 10^{-1} \pm 5.49 \times 10^{-4}$	$4.19 \times 10^{-1} \pm 6.51 \times 10^{-3}$	Not reported
Usability			
Parameter adjustability	High (12+ parameters)	Limited	Moderate (4 parameters)
User interface	Graphical with visualization	Command line	Semi-automated macro
Availability	Open-source	Limited availability	Open-source
Installation complexity	Moderate	High (requires MATLAB)	Low (ImageJ macro)
Output			
Generated outputs	CSV data, processed images, graphs	Processed images	CSV data
Real-time visualization	Yes	No	No

starting point for accurate wound detection across various imaging conditions. Other detection tools were unable to account for these cells in their calculations, suggesting that our tool is one of the few freely available options that offer such high precision in wound area closure detection. Additionally, other tools failed to detect empty regions occasionally, leading to inaccurate wound area detection. CSMA also outperforms others in terms of image processing speed. For example, while HTM takes about $4.19 \times 10^{-1} \pm 6.51 \times 10^{-3}$ seconds to process an image, CSMA requires only $2.26 \times 10^{-1} \pm 5.49 \times 10^{-4}$ second with default settings. These processing speed measurements were obtained using Intel Xeon Gold 6244 Dual CPU, @ 3.60GHz 256GB RAM, NVIDIA QUadro RTX 6000 operating on Windows 11 Pro for Workstations. For large-scale datasets, GPU acceleration could be explored in future implementations to further reduce processing time, as many of the image processing operations in CSMA are highly parallelizable and would benefit from GPU optimization.

Understanding the limitations of each analysis tool is essential for interpreting performance differences. HTM primarily detects only the largest connected wound region, causing underestimation when wounds fragment, particularly with individually migrating cells. MRI struggles with detecting intra-wound cells and often overestimates wound fronts due to its variance-based method, which affects low-contrast regions. Both tools fail to detect empty regions in disconnected wounds, critically impacting closure rate accuracy. While CSMA addresses these major limitations, it still faces challenges with the corrections of field-of-view shifts and illumination changes, though parameter adjustments can mitigate these issues. All three tools use threshold-based approaches, introducing some inherent subjectivity in boundary determination—a consideration when selecting an analysis method for specific experimental conditions.

The datasets used for testing the effect of various VDR agonists on SW480-ADH migration were more difficult to analyze for several reasons. First, uneven and constantly changing illumination impeded edge detection because the borders of dark and light regions were detected as the wound edges by the Canny method, which is based on detecting the regions of sharp illumination changes [22]. This drawback was minimized by carefully adjusting the contrast limit and square grid size. Increasing the contrast limit and decreasing the square grid size improved the detection of smaller elements, such as single cells, while decreasing the contrast limit and increasing the square grid size helped to reduce the detection of false edges.

In addition, it is occasionally possible for the ''field of view'' and the ''location of the wound in the image'' to be slightly shifted as a result of the image stitching process or a minor disturbance of the imaging device inside the incubator during the image acquisition procedure. Since the CSMA tool applies the mask from the previous image to the current one, this shift resulted in an inaccurate wound detection with the default parameters. However, this limitation was overcome by increasing the mask erosion parameter. It is advised to accompany such adjustments with increasing the dilation radius to maintain accurate detection of the true wound edges. Lastly, the microscope's focus likely shifted over time, causing cells inside and at the front of the wound to appear larger and blurrier in later images. Although the resulting sudden drops in the wound area could not be entirely corrected, CSMA still accurately detected small elements and wound edges.

While CSMA's adjustable parameters provide flexibility, this customizability has potential limitations. Analysis quality depends on appropriate parameter selection, which may require trial and error and introduce some subjectivity. To overcome this, we provide well-performing default

parameters and guidelines for adjustment in the README file. The visual output allows validation of parameter choices against original images. Parameter customization could impact reproducibility between laboratories if not documented, so we recommend reporting all adjusted parameters (as shown in Table 2) to ensure transparency. Overall, the benefits of parameter adjustability in handling diverse experimental conditions outweigh these potential limitations.

Precise detection of wound edges and cells within the wound allowed CSMA to achieve high-accuracy area detection and produce smooth wound closure curves. As a consequence, wound closure curves generated by CSMA fit the linear and exponential models better than those generated by HTM and MRI (Supplementary Fig. S4). Although both the linear and exponential regression curves have R^2 values above 0.90, the exponential regression curve is more suitable due to its higher R^2 value. This is because exponential curves can accurately fit both visually linear and exponential wound closure patterns, whereas the linear fit aligns well only in cases of linear closure. For example, as demonstrated in Fig. 4 and 5, a single linear fit line cannot adequately describe the cell behavior over the entire period since different time intervals exhibit varying closure speeds. Therefore, two linear trendlines are required to capture the true behavior of this curve, which is both time-consuming and potentially misleading. In contrast, a single exponential decay curve fits the data well and allows the behavior to be described with only one decay rate.

One limitation of the study is the inconsistency in the initial wound width due to variations in the force applied to the pipette tip. However, these variations are compensated through the use of normalization (Equation 1), which expresses closure as a percentage of initial area, enabling valid comparisons between experiments with different starting sizes. The exponential decay model further accommodates different initial conditions by characterizing proportional rather than absolute closure rates. It should be noted that extreme width variations might still influence closure dynamics by affecting cell density at wound edges or migration distances. We minimized these effects through consistent wound creation technique and multiple replicates per condition. Additional challenges include low image quality, cells with suboptimal adhesion properties such as being overly adhesive or non-adhesive, number of adjustable parameters, and potential installation issues due to operating system differences and unique user settings.

Though CSMA offers two modes of wound closure quantification, we found that the area quantification method was more accurate than width because it accounted for cells proliferating in the middle of the gap.

FUTURE DIRECTIONS

Future improvements of CSMA may explore several directions that build upon its current capabilities. First, integration of deep learning approaches could improve the precision of cell detection under challenging conditions. Specifically, convolutional neural networks or U-Net architectures that have been successful in biomedical image segmentation could help detect low-contrast cells or incomplete wound edges [28], [29], [30]. These approaches would be particularly valuable for analyzing images with poor illumination or high noise levels. Second, implementing adaptive parameter optimization [31], [32] may reduce manual tuning requirements and improve reproducibility. This may involve the development of algorithms that automatically adjust parameters based on image characteristics such as resolution, contrast, and noise levels. Multi-scale processing techniques [33] could better accommodate irregular wound geometries and varying cell morphologies across different experimental conditions. Third, enhancing CSMA with interactive features would further improve usability. This might include visualization of parameter adjustment in real time, automatic parameter recommendation based on image quality metrics, and interactive correction tools that allow users to refine the boundaries detected when needed. Lastly, the development of metaheuristic algorithms [34], [35], [36] to automatically determine optimal parameter settings based on image characteristics may provide additional benefits. Such automation would minimize user intervention and potentially improve reproducibility across different experimental setups, particularly when analyzing large datasets from diverse imaging conditions.

V. CONCLUSION

Our study demonstrates that the newly developed CSMA tool offers a significant advancement in the accurate quantification of wound closure in cell migration assays. By addressing the limitations of existing methods, which often fail to detect cells within the wound gap and result in biased measurements, our tool provides a more reliable and precise approach for evaluating cell migration and wound healing. The ability of our tool to identify empty regions and avoid overestimation of the cell-covered area further validates its effectiveness. Additionally, accurately detecting wound closure at all time points allows for the correct estimation of wound closure dynamics such as its rate. This innovative solution not only enhances the accuracy of wound closure assessments but also offers a user-friendly platform for researchers to obtain robust and reproducible results in cell migration studies such as in studying the metastatic properties of cancer cell lines.

COMPETING INTERESTS

No competing interest is declared.

AUTHOR CONTRIBUTIONS STATEMENT

T.T.P.: Conceptualization, Funding acquisition, Supervision, Writing – review & editing, A.S.: Formal analysis, Software, Writing – original draft, T.E.: Formal analysis, Software, Writing – review & editing, Z.O.: Writing – review & editing, F.M.: Conceptualization, Funding acquisition, Supervision, Visualization, Writing – review & editing.

SUPPLEMENTARY DATA

Supplementary data are available at **IEEE** *Access* online.

ACKNOWLEDGMENT

The authors extend their sincere gratitude to Daniyar Kakimbekov from the Department of Computer Science at Nazarbayev University for his invaluable advice and support throughout this project. *(Tri Thanh Pham and Amina Sagymbayeva contributed equally to this work.)*

AVAILABILITY AND IMPLEMENTATION

CSMA is available as a standalone and ImageJ-compatible tool with its source code at https://github.com/AminaSagymbayeva/CSMA_WoundHealing

REFERENCES

[1] C.-C. Liang, A. Y. Park, and J.-L. Guan, "in vitro scratch assay: A convenient and inexpensive method for analysis of cell migration in vitro," *Nature Protocols*, vol. 2, no. 2, pp. 329–333, Feb. 2007.

[2] J. E. N. Jonkman, J. A. Cathcart, F. Xu, M. E. Bartolini, J. E. Amon, K. M. Stevens, and P. Colarusso, "An introduction to the wound healing assay using live-cell microscopy," *Cell Adhes. Migration*, vol. 8, no. 5, pp. 440–451, Sep. 2014.

[3] P. Friedl and D. Gilmour, "Collective cell migration in morphogenesis, regeneration and cancer," *Nature Rev. Mol. Cell Biol.*, vol. 10, no. 7, pp. 445–457, Jul. 2009.

[4] C. D. Nobes and A. Hall, "Rho GTPases control polarity, protrusion, and adhesion during cell movement," *J. Cell Biol.*, vol. 144, no. 6, pp. 1235–1244, Mar. 1999, doi: 10.1083/jcb.144.6.1235.

[5] J. Y. Ng, X. Zhu, D. Mukherjee, C. Zhang, S. Hong, Y. Kumar, R. Gokhale, and P. L. R. Ee, "Pristine gellan gum–collagen interpenetrating network hydrogels as mechanically enhanced anti-inflammatory biologic wound dressings for burn wound therapy," *ACS Appl. Bio Mater.*, vol. 4, no. 2, pp. 1470–1482, Feb. 2021.

[6] M. Mirzahosseinipour, K. Khorsandi, R. Hosseinzadeh, M. Ghazaeian, and F. K. Shahidi, "Antimicrobial photodynamic and wound healing activity of curcumin encapsulated in silica nanoparticles," *Photodiagnosis Photodynamic Therapy*, vol. 29, Mar. 2020, Art. no. 101639, doi: 10.1016/j.pdpdt.2019.101639.

[7] O. Ilina and P. Friedl, "Mechanisms of collective cell migration at a glance," *J. Cell Sci.*, vol. 122, no. 18, pp. 3203–3208, Sep. 2009, doi: 10.1242/jcs.036525.

[8] N. Lecomte, J. T. Njardarson, P. Nagorny, G. Yang, R. Downey, O. Ouerfelli, M. A. S. Moore, and S. J. Danishefsky, "Emergence of potent inhibitors of metastasis in lung cancer via syntheses based on migrastatin," *Proc. Nat. Acad. Sci. USA*, vol. 108, no. 37, pp. 15074–15078, Aug. 2011, doi: 10.1073/pnas.1015247108.

[9] C. Hafner, "Ephrin-B2 is differentially expressed in the intestinal epithelium in Crohn's disease and contributes to accelerated epithelial wound healingin vitro," *World J. Gastroenterology*, vol. 11, no. 26, p. 4024, 2005, doi: 10.3748/wjg.v11.i26.4024.

[10] R. Farooqui and G. Fenteany, "Multiple rows of cells behind an epithelial wound edge extend cryptic lamellipodia to collectively drive cell-sheet movement," *J. Cell Sci.*, vol. 118, no. 1, pp. 51–63, Jan. 2005, doi: 10.1242/jcs.01577.

[11] N. S. Ariffin, "The CellProfiler pipeline analysis of cell migration," *Acta Histochemica*, vol. 125, no. 7, Oct. 2023, Art. no. 152074, doi: 10.1016/j.acthis.2023.152074.

[12] A. Suarez-Arnedo, F. Torres Figueroa, C. Clavijo, P. Arbeláez, J. C. Cruz, and C. Muñoz-Camargo, "An image j plugin for the high throughput image analysis of in vitro scratch wound healing assays," *PLoS ONE*, vol. 15, no. 7, Jul. 2020, Art. no. e0232565, doi: 10.1371/journal.pone.0232565.

[13] J. P. Silva Nunes and A. A. Martins Dias, "ImageJ macros for the user-friendly analysis of soft-agar and wound-healing assays," *BioTechniques*, vol. 62, no. 4, pp. 175–179, Apr. 2017, doi: 10.2144/000114535.

[14] A. V. P. Bobadilla, J. Arévalo, E. Sarró, H. M. Byrne, P. K. Maini, T. Carraro, S. Balocco, A. Meseguer, and T. Alarcón, "in vitro cell migration quantification method for scratch assays," *J. Roy. Soc. Interface*, vol. 16, no. 151, Feb. 2019, Art. no. 20180709, doi: 10.1098/rsif.2018.0709.

[15] T. Gebäck, M. M. P. Schulz, P. Koumoutsakos, and M. Detmar, "TScratch: A novel and simple software tool for automated analysis of monolayer wound healing assays: Short technical reports," *BioTechniques*, vol. 46, no. 4, pp. 265–274, Apr. 2009, doi: 10.2144/000113083.

[16] F. Garcia-Fossa, V. Gaal, and M. B. de Jesus, "PyScratch: An ease of use tool for analysis of scratch assays," *Comput. Methods Programs Biomed.*, vol. 193, Sep. 2020, Art. no. 105476, doi: 10.1016/j.cmpb.2020.105476.

[17] A. Vargas, M. Angeli, C. Pastrello, R. McQuaid, H. Li, A. Jurisicova, and I. Jurisica, "Robust quantitative scratch assay," *Bioinformatics*, vol. 32, no. 9, pp. 1439–1440, May 2016, doi: 10.1093/bioinformatics/btv746.

[18] M. Cortesi, A. Pasini, A. Tesei, and E. Giordano, "AIM: A computational tool for the automatic quantification of scratch wound healing assays," *Appl. Sci.*, vol. 7, no. 12, p. 1237, Nov. 2017, doi: 10.3390/app7121237.

[19] C. A. Schneider, W. S. Rasband, and K. W. Eliceiri, "NIH image to ImageJ: 25 years of image analysis," *Nature Methods*, vol. 9, no. 7, pp. 671–675, Jul. 2012.

[20] H. G. Pálmer, J. M. González-Sancho, J. Espada, M. T. Berciano, I. Puig, J. Baulida, M. Quintanilla, A. Cano, A. G. de Herreros, and M. Lafarga, "Vitamin D_3 promotes the differentiation of colon carcinoma cells by the induction of e-cadherin and the inhibition of β-catenin signaling," *J. Cell Biol.*, vol. 154, no. 2, pp. 369–388, 2001.

[21] S. M. Pizer, E. P. Amburn, J. D. Austin, R. Cromartie, A. Geselowitz, T. Greer, B. T. H. Romeny, J. B. Zimmerman, and K. Zuiderveld, "Adaptive histogram equalization and its variations," *Comput. Vis., Graph., Image Process.*, vol. 39, no. 3, pp. 355–368, Sep. 1987, doi: 10.1016/s0734-189x(87)80186-x.

[22] L. Xuan and Z. Hong, "An improved Canny edge detection algorithm," in *Proc. 8th IEEE Int. Conf. Softw. Eng. Service Sci. (ICSESS)*, Nov. 2017, pp. 275–278, doi: 10.1109/ICSESS.2017.8342913.

[23] N. Otsu, "A threshold selection method from gray-level histograms," *IEEE Trans. Syst., Man, Cybern.*, vol. SMC-9, no. 1, pp. 62–66, Jan. 1979, doi: 10.1109/TSMC.1979.4310076.

[24] V. Baecker, "ImageJ macro tool sets for biological image analysis," in *Proc. ImageJ User Developer Conf.*, vol. 24, 2012, p. 26.

[25] V. Bäcker. (2002). *MRI Wound Healing Tool*. Accessed: Nov. 30, 2023. [Online]. Available: https://github.com/MontpellierRessourcesImagerie/imagej_macros_and_scripts/wiki/Wound-Healing-Tool

[26] H. M. Byrne and M. A. J. Chaplain, "Growth of necrotic tumors in the presence and absence of inhibitors," *Math. Biosci.*, vol. 135, no. 2, pp. 187–216, Jul. 1996.

[27] M. Poujade, E. Grasland-Mongrain, A. Hertzog, J. Jouanneau, P. Chavrier, B. Ladoux, A. Buguin, and P. Silberzan, "Collective migration of an epithelial monolayer in response to a model wound," *Proc. Nat. Acad. Sci. USA*, vol. 104, no. 41, pp. 15988–15993, Oct. 2007.

[28] O. Ronneberger, P. Fischer, and T. Brox, "U-Net: Convolutional networks for biomedical image segmentation," in *Proc. 18th Int. Conf. Med. Image Comput. Comput.-Assist. Intervent. (MICCAI)*, Munich, Germany. Cham, Switzerland: Springer, Jan. 2015, pp. 234–241.

[29] J. Long, E. Shelhamer, and T. Darrell, "Fully convolutional networks for semantic segmentation," in *Proc. IEEE Conf. Comput. Vis. Pattern Recognit. (CVPR)*, Jun. 2015, pp. 3431–3440.

[30] D. A. Van Valen, T. Kudo, K. M. Lane, D. N. Macklin, N. T. Quach, M. M. DeFelice, I. Maayan, Y. Tanouchi, E. A. Ashley, and M. W. Covert, "Deep learning automates the quantitative analysis of individual cells in live-cell imaging experiments," *PLOS Comput. Biol.*, vol. 12, no. 11, Nov. 2016, Art. no. e1005177.

[31] N. Otsu, "A threshold selection method from gray-level histograms," *Automatica*, vol. 11, nos. 285–296, pp. 23–27, Jan. 1975.

[32] W.-H. Tsai, "Moment-preserving thresolding: A new approach," *Comput. Vis., Graph., Image Process.*, vol. 29, no. 3, pp. 377–393, Mar. 1985.

[33] T. Lindeberg, "Scale-space theory: A basic tool for analyzing structures at different scales," *J. Appl. Statist.*, vol. 21, nos. 1–2, pp. 225–270, Jan. 1994.

[34] J. Kennedy and R. C. Eberhart, "Particle swarm optimization," in *Proc. Int. Conf. neural Netw.*, vol. 4, Nov. 2002, pp. 1942–1948.

[35] P. Siarry and G. Berthiau, "Fitting of Tabu search to optimize functions of continuous variables," *Int. J. Numer. Methods Eng.*, vol. 40, no. 13, pp. 2449–2457, Jul. 1997.
[36] X. Yang, "A new metaheuristic bat-inspired algorithm," in *Nature Inspired Cooperative Strategies for Optimization (NICSO 2010)*. Cham, Switzerland: Springer, Jan. 2010, pp. 65–74.

TRI THANH PHAM received the double degree in advanced science (mathematics and physics) and aerospace engineering from The University of Sydney, Australia, and the Ph.D. degree in computational biophysics from Monash University, Australia. After stints in USA and Switzerland (where he received a prestigious award from the Swiss National Science Foundation), he joined Nazarbayev University, as an Assistant Professor with the Department of Biology, in August 2019. He has over 22 years of experience with computational simulations and at least 13 years of experience with live-cell imaging and biophysical measurements using optical and atomic force microscopes. He recently established the Mechanobiology Laboratory to investigate changes in mammalian and bacterial cell biophysical properties, viability, and biofilm formation when they interact with therapeutic drugs, antibiotics, nanoparticles, bio/nanomaterials, and material surfaces, such as metal implants or polymer scaffolds.

AMINA SAGYMBAYEVA is currently pursuing the B.Sc. degree in biological sciences with Nazarbayev University, Astana, Kazakhstan. Her current research interests include environmental policy and water conservation.

TIMUR ELEBESSOV received the B.Sc. degree in natural sciences from Al-Farabi Kazakh National University, Almaty, Kazakhstan, and the M.Sc. degree in biological sciences from Nazarbayev University, Astana, Kazakhstan, in September 2022, where he is currently pursuing the Ph.D. degree. His research interests include biophysics and nanoparticles characterization.

ZHADYRA ONZHANOVA received the B.Sc. and M.Sc. degrees from L. N. Gumilyov Eurasian National University, Astana, Kazakhstan, in 2011 and 2015, respectively, and the M.Sc. degree from Joseph Fourier University, Grenoble, France, in 2016. She is currently pursuing the Ph.D. degree with Nazarbayev University, Astana. Her research interests include biochemistry, drug discovery, molecular biology of cancer, and neuroscience.

FERDINAND MOLNÁR (Associate Member, IEEE) received the M.Sc. degree in biochemistry from Comenius University, Bratislava, Slovakia, in 2001, and the Ph.D. degree in biochemistry (minor in pharmacology and bioinformatics) from the University of Kuopio, Kuopio, Finland, in 2006. From 2006 to 2008, he was a Post-Doctoral Researcher with the Institute of Genetics and Molecular and Cellular Biology, Illkirch, France. In 2008, he returned to Finland and held various positions at the University of Eastern Finland, Kuopio. Before joining Nazarbayev University, as an Associate Professor with the Department of Biology, in 2018, he held a position of Senior Researcher and the Laboratory Head of the University of Eastern Finland. His current research interests include structural and chemical biology, chem-bio informatics, drug discovery, and ML in chemistry.